

Supporting Information for

## Low-temperature Growing Anatase-TiO<sub>2</sub>/SnO<sub>2</sub> Multi-dimensional Heterojunctions at MXene Conductive Network for High-efficient Perovskite Solar Cells

Linsheng Huang<sup>1</sup>, Xiaowen Zhou<sup>1</sup>, Rui Xue<sup>1</sup>, Pengfei Xu<sup>1</sup>, Siliang Wang<sup>1</sup>, Chao Xu<sup>1</sup>, Wei Zeng<sup>1, \*</sup>, Yi Xiong<sup>2, 3, \*</sup>, Hongqian Sang<sup>3, 4</sup>, Dong Liang<sup>1</sup>

<sup>1</sup>National Engineering Research Center for Agro-Ecological Big Data Analysis & Application, School of Electronics and Information Engineering, Anhui University, No.111 Jiulong Road, Hefei 230601, People's Republic of China

<sup>2</sup>Science and Technology Institute, Hubei Key Laboratory of Biomass Fibers & Eco-Dyeing & Finishing, Wuhan Textile University, Wuhan 430073, People's Republic of China

<sup>3</sup>School of Physics and Technology, MOE Key Laboratory of Artificial Micro- and Nano-Structures and Center for Electron Microscopy, Wuhan University, Wuhan 430072, People's Republic of China

<sup>4</sup>Department of Physics, King's College London, The Strand, London WC2R 2LS, United Kingdom

\*Corresponding authors. E-mail: youfmail@163.com (Wei Zeng); xiong@wtu.edu.cn or xiongyi@whu.edu.cn (Yi Xiong)

### Supplementary Figures

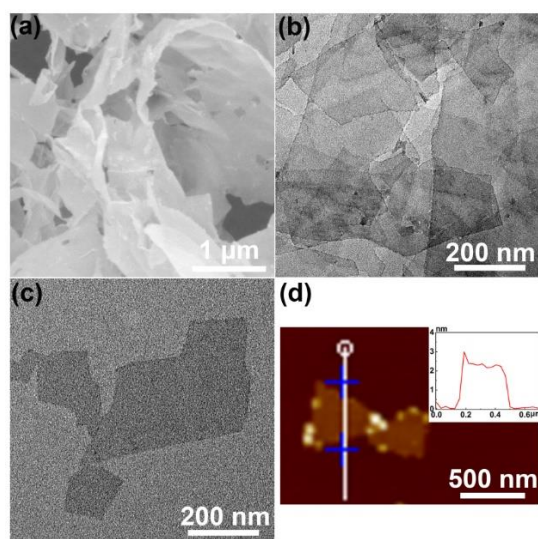


**Fig. S1** (a) The SEM morphology, (b-c) TEM morphologies, and (d) AFM surface morphology of resulted MXene material with its height profile in inset

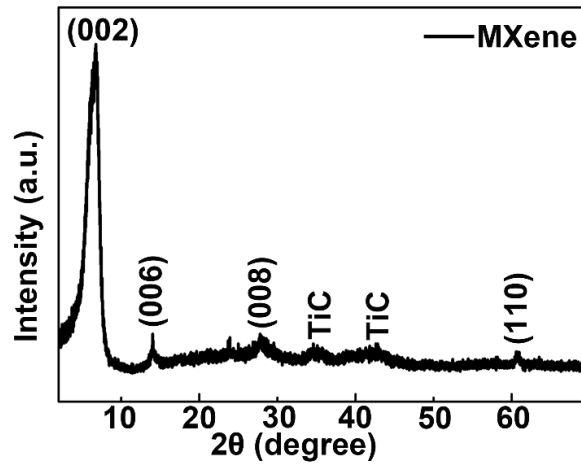


Fig. S2 XRD pattern of resulted MXene material

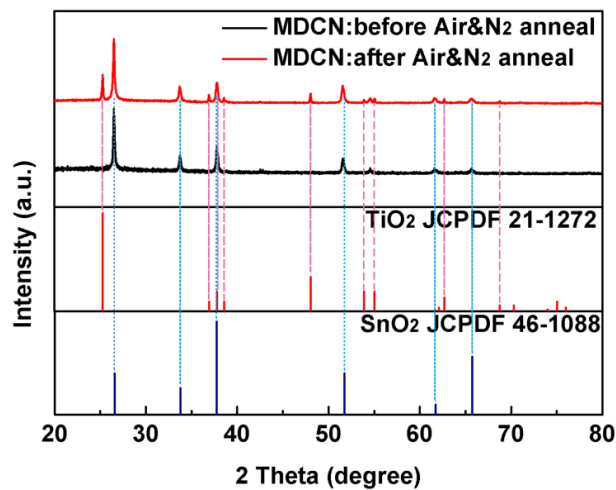


Fig. S3 XRD patterns of MDCN before and after controlled anneal method in Air&N<sub>2</sub> atmospheres

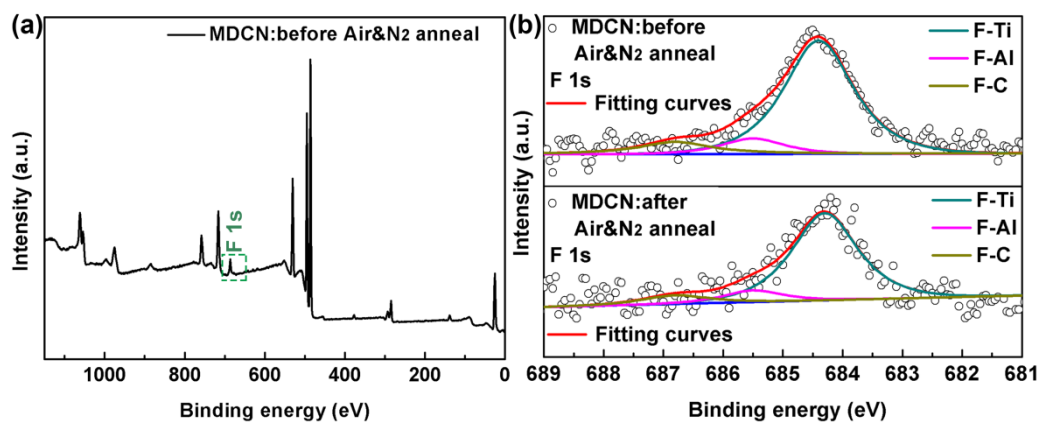


Fig. S4 **a** The survey spectra of MDCN before controlled anneal. **b** The extracted F 1s spectra of MDCN samples before and after controlled anneal

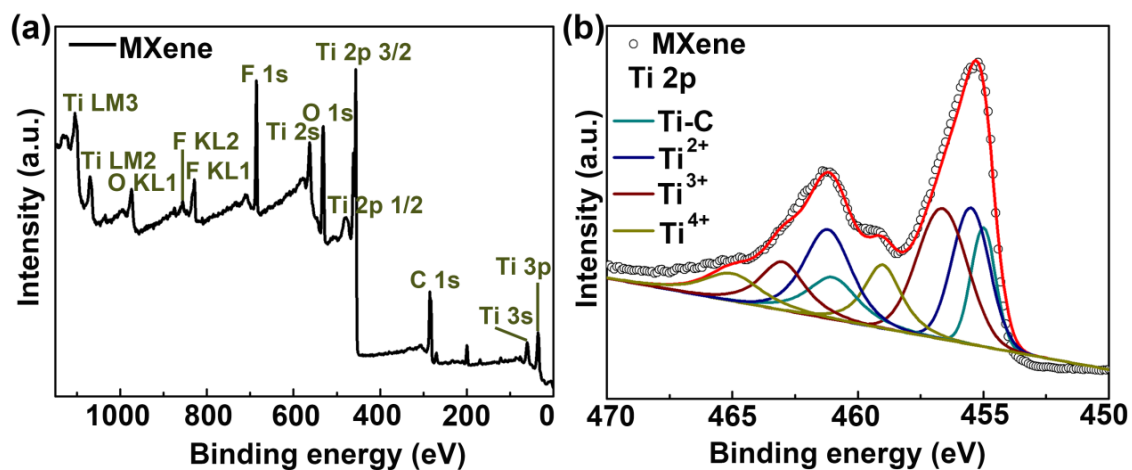


Fig. S5 Survey spectrum of **a** pure MXene **b** with its Ti 2p

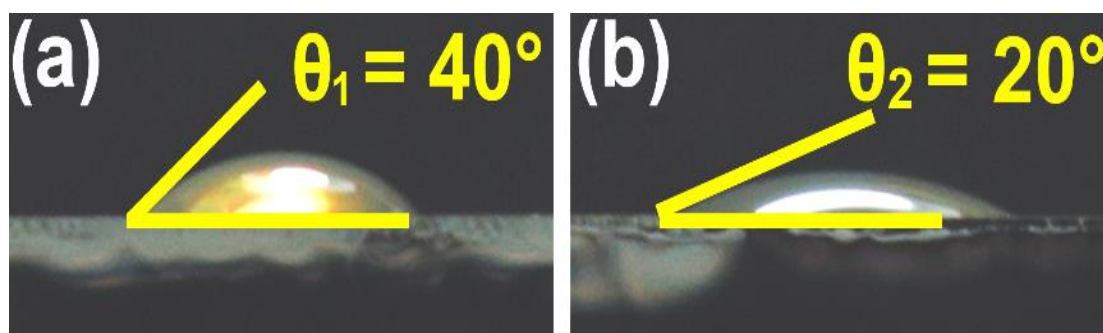


Fig. S6 Wetting angles of a water droplet on the **(a)** SnO<sub>2</sub> and **(b)** MDCN films

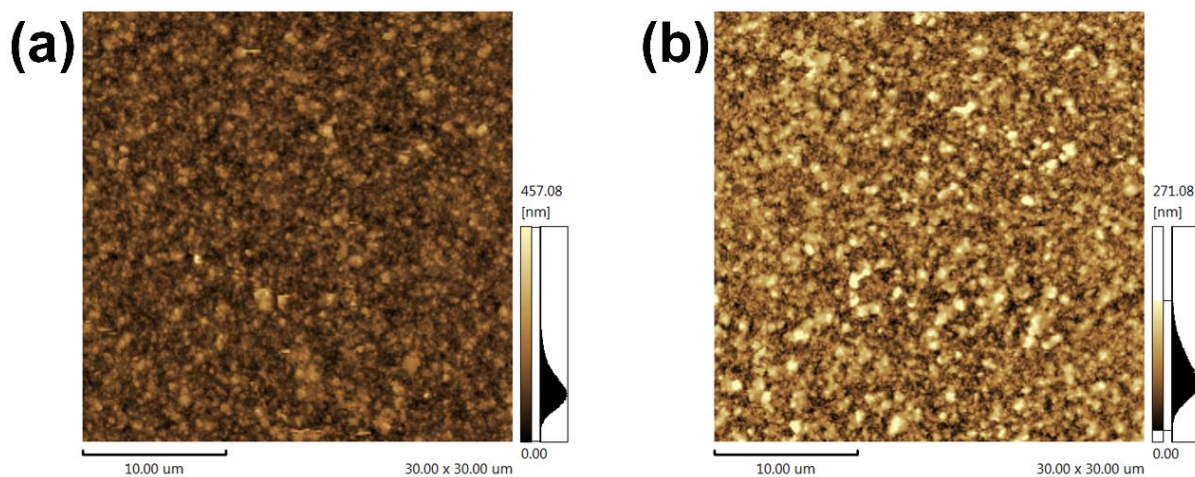
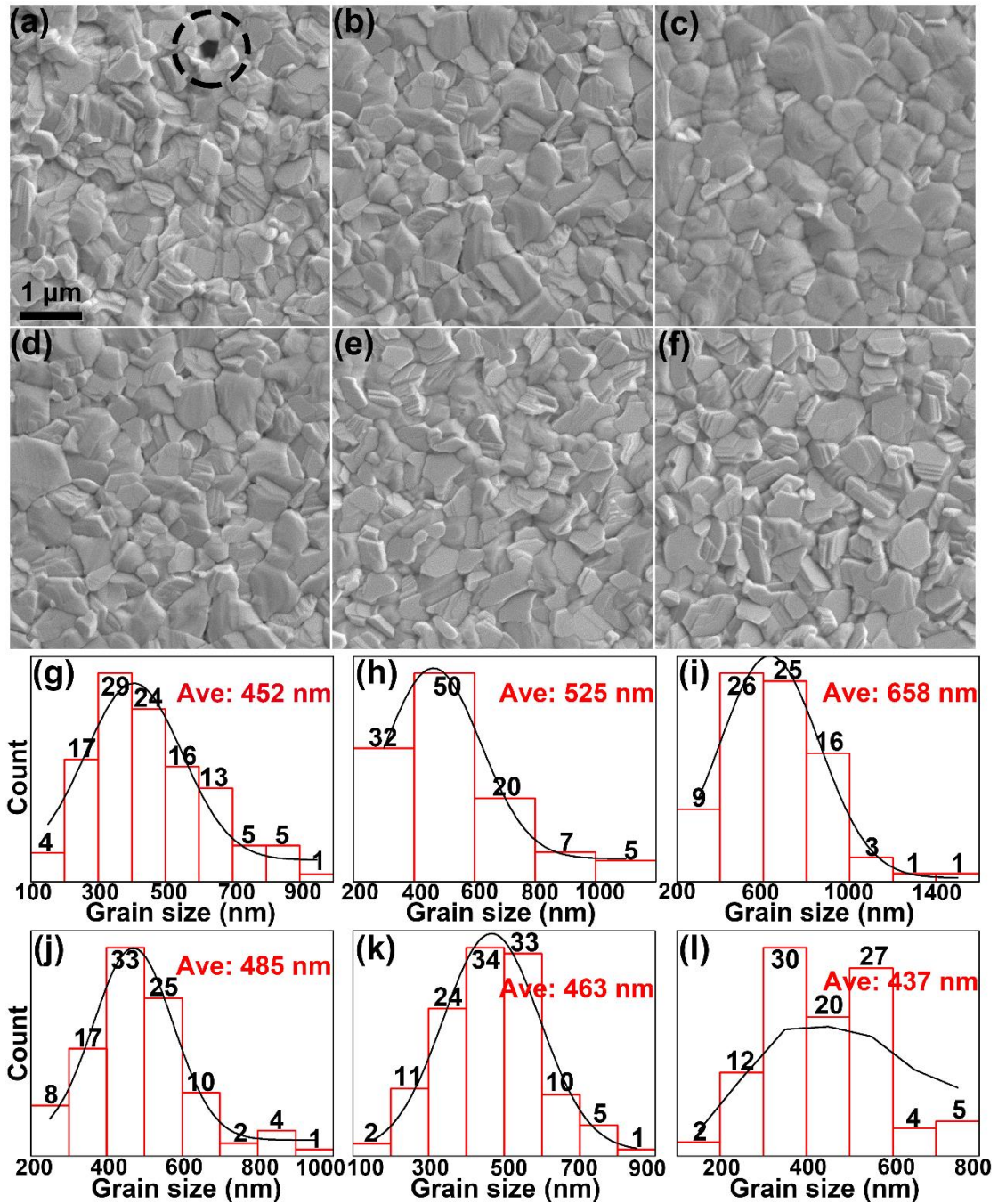
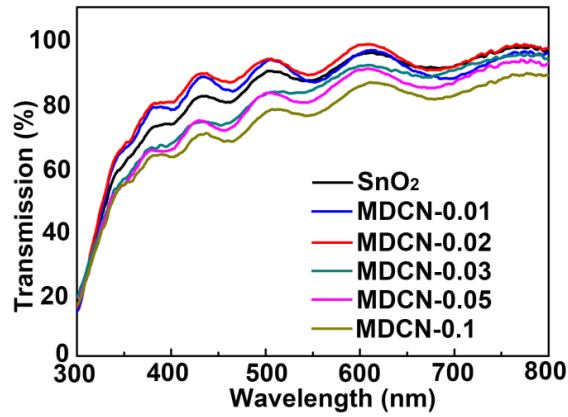


Fig. S7 AFM images of **(a)** SnO<sub>2</sub> and **(b)** MDCN surfaces



**Fig. S8** Top-view SEM images of perovskite/ETL/FTO with different ETL: (a) SnO<sub>2</sub>; (b) MDCN-0.01; (c) MDCN-0.02 (i.e., MDCN sample); (d) MDCN-0.03; (e) MDCN-0.05; (f) MDCN-0.1. (g-l) Statistic grain size distributions for perovskite film in (a-f)



**Fig. S9** Transmittance spectra of SnO<sub>2</sub>, MDCN-0.01, MDCN-0.02, MDCN-0.03, MDCN-0.05, and MDCN-0.1 ETLs

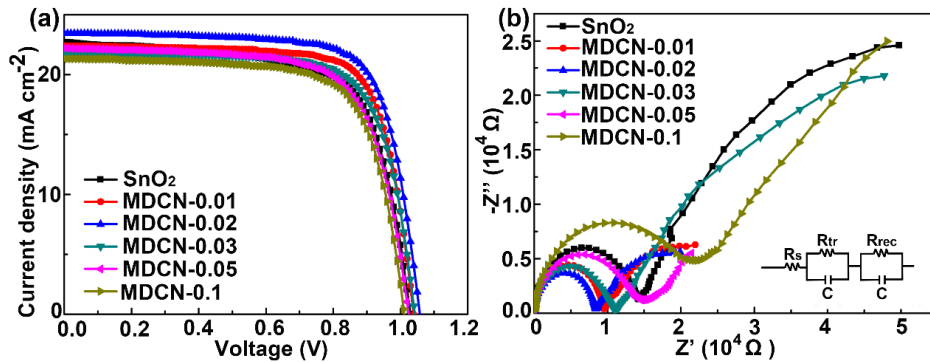


**Fig. S10** (a) J-V curves and (b) Nyquist plots of EIS for PSCs using SnO<sub>2</sub>, MDCN-0.01, MDCN-0.02, MDCN-0.03, MDCN-0.05, and MDCN-0.1 as ETLs. The equivalent circuit for (b) shown its inset.

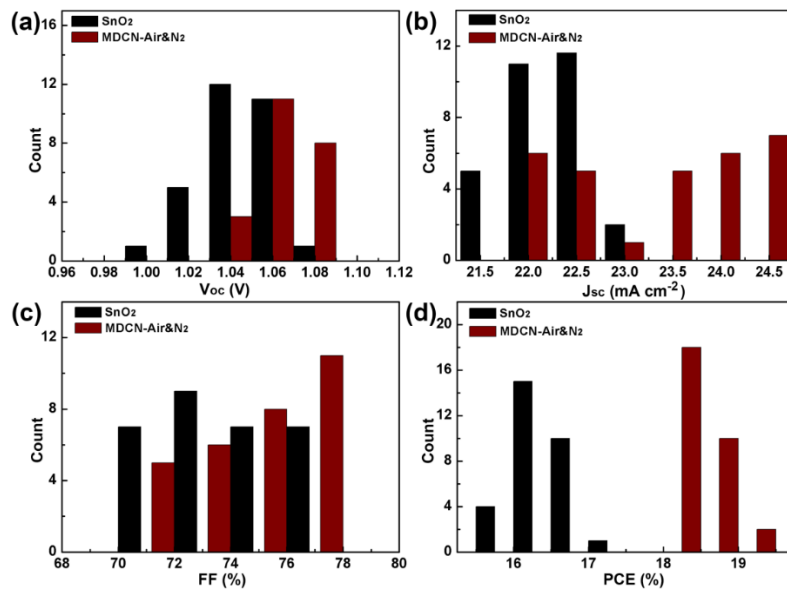


**Fig. S11** Histogram of parameters of PSCs with SnO<sub>2</sub> and MDCN-Air&N<sub>2</sub> ETLs

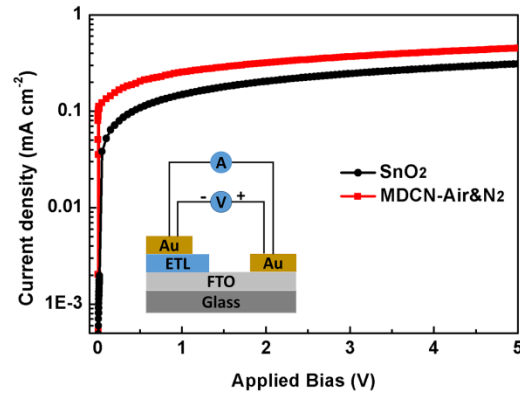


**Fig. S12** The SCLC curve of SnO<sub>2</sub> and MDCN-Air&N<sub>2</sub> layers with the test devices sketch in inset

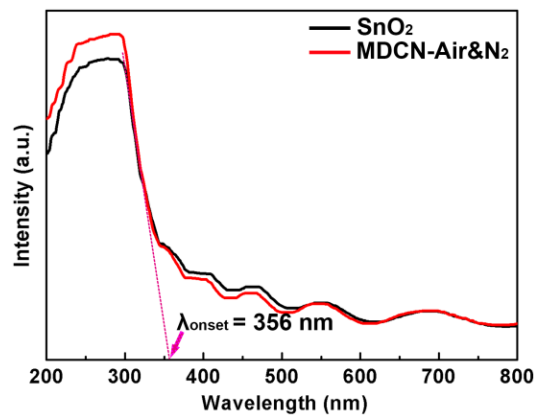


**Fig. S13** Absorption onset value measure for SnO<sub>2</sub> and MDCN-Air&N<sub>2</sub> samples with UV-vis absorption spectra

**Table S1** Atomic contents of different Ti-based bonds for pure MXene and MDCN

	Ti-C	Ti <sup>2+</sup>	Ti <sup>3+</sup>	Ti <sup>4+</sup>
Pure MXene	18.76	33.91	31.67	15.65
MDCN	19.94	31.27	25.39	23.40

**Table S2** Device performance of PSCs based on ETLs with different MXene contents (30 samples for each type of ETL)

ETL	$V_{oc}$ (V)	$J_{sc}$ (mA cm <sup>-2</sup> )	$FF$ (%)	PCE (%)
SnO <sub>2</sub>	1.03 ± 0.04	22.51 ± 1.56	70.55 ± 3.11	16.42 ± 0.41
MDCN-0.01	1.05 ± 0.05	22.73 ± 1.65	72.89 ± 3.50	17.38 ± 0.48
MDCN-0.02	1.07 ± 0.03	23.13 ± 1.39	74.62 ± 3.35	18.44 ± 0.70
MDCN-0.03	1.04 ± 0.05	21.92 ± 0.76	73.14 ± 2.88	16.74 ± 0.24
MDCN-0.05	1.03 ± 0.06	22.33 ± 1.79	69.51 ± 3.84	15.93 ± 0.82
MDCN-0.1	1.02 ± 0.04	21.76 ± 0.74	69.71 ± 3.04	15.54 ± 0.44